

# Conformational Properties of Peptides Corresponding to the Ebola virus GP2 Membrane-Proximal External Region in the Presence of Micelle-Forming Surfactants and Lipids

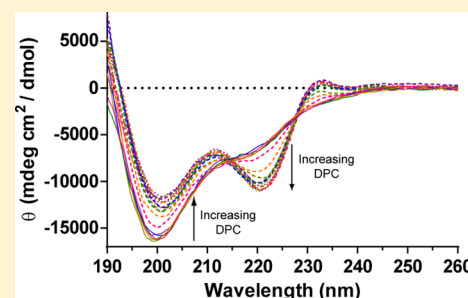
Lauren K. Regula,<sup>†</sup> Richard Harris,<sup>†</sup> Fang Wang,<sup>§</sup> Chelsea D. Higgins,<sup>†</sup> Jayne F. Koellhoffer,<sup>†</sup> Yue Zhao,<sup>§</sup> Kartik Chandran,<sup>‡</sup> Jianmin Gao,<sup>§</sup> Mark E. Girvin,<sup>†</sup> and Jonathan R. Lai<sup>\*,†</sup>

<sup>†</sup>Department of Biochemistry and <sup>‡</sup>Department of Microbiology and Immunology, Albert Einstein College of Medicine, 1300 Morris Park Avenue, Bronx, New York 10461, United States

<sup>§</sup>Department of Chemistry, Boston College, 140 Commonwealth Avenue, Chestnut Hill, Massachusetts 02467, United States

## Supporting Information

**ABSTRACT:** Ebola virus and Sudan virus are members of the family *Filoviridae* of nonsegmented negative-strand RNA viruses (“filoviruses”) that cause severe hemorrhagic fever with fatality rates as high as 90%. Infection by filoviruses requires membrane fusion between the host and the virus; this process is facilitated by the two subunits of the envelope glycoprotein, GP1 (the surface subunit) and GP2 (the transmembrane subunit). The membrane-proximal external region (MPER) is a Trp-rich segment that immediately precedes the transmembrane domain of GP2. In the analogous glycoprotein for HIV-1 (gp41), the MPER is critical for membrane fusion and is the target of several neutralizing antibodies. However, the role of the MPER in filovirus GP2 and its importance in membrane fusion have not been established. Here, we characterize the conformational properties of peptides representing the GP MPER segments of Ebola virus and Sudan virus in the presence of micelle-forming surfactants and lipids, at pH 7 and 4.6. Circular dichroism spectroscopy and tryptophan fluorescence indicate that the GP2 MPER peptides bind to micelles of sodium dodecyl sulfate and dodecylphosphocholine (DPC). Nuclear magnetic resonance spectroscopy of the Sudan virus MPER peptide revealed that residues 644–651 interact directly with DPC, and that this interaction enhances the helical conformation of the peptide. The Sudan virus MPER peptide was found to moderately inhibit cell entry by a GP-pseudotyped vesicular stomatitis virus but did not induce leakage of a fluorescent molecule from a large unilamellar vesicle comprised of 1-palmitoyl-2-oleoylphosphatidylcholine or cause hemolysis. Taken together, this analysis suggests the filovirus GP2 MPER binds and inserts shallowly into lipid membranes.



Members of the family *Filoviridae* of nonsegmented negative-strand RNA viruses are taxonomically classified into two genera, *Ebolavirus* and *Marburgvirus* (“filoviruses”).<sup>1,2</sup> Two prototypic ebolaviruses, Ebola virus (EBOV) and Sudan virus (SUDV), were first identified in 1976 when outbreaks occurred in Zaire (known today as the Democratic Republic of Congo) and Sudan. Filovirus infection causes severe hemorrhagic fever; EBOV and SUDV infections have been associated with high fatality rates (50–90% in some outbreaks).<sup>3–5</sup>

Filoviruses enter cells using “class I” viral fusion proteins, defined by the formation of an  $\alpha$ -helical six-helix bundle by the glycoprotein ectodomain.<sup>6–8</sup> GP is the envelope glycoprotein and consists of GP1 and GP2, the receptor-binding and fusion subunits, respectively.<sup>9,10</sup> GP1 and GP2 are generated from the GP precursor by furin cleavage and remain associated on the refusion spike via disulfide bonds.<sup>10</sup>

EBOV entry, which has been well-characterized, is initiated by binding of GP1 to adherence factors and uptake of the viral particle into the endosome.<sup>11</sup> Once in the endosome, host cysteine proteases cathepsins L and B proteolytically cleave GP1 removing all but an ~17 kDa fragment.<sup>12</sup> This cleavage

event is thought to expose a receptor-binding domain (RBD) on GP1 that engages a putative host receptor, the endosomal cholesterol transporter Niemann-Pick C1 (NPC-1), to trigger membrane fusion.<sup>13–16</sup> Next, the fusion loop (FL) of GP2 inserts into the endosomal membrane, leading to an extended intermediate conformation in which GP2 spans both viral and host endosomal membranes.<sup>6,7</sup> The heptad repeat regions of GP2 then fold into the highly stable six-helix bundle that brings the viral and host membranes into the proximity of each other.<sup>17–19</sup> The energy released from this folding event is thought to lower the kinetic barrier for membrane fusion, similar to other class I glycoproteins such as those from HIV-1 and influenza.<sup>6,7</sup> Presumably, this folding event yields a “hemifusion” intermediate in which the outer leaflets of the two bilayers are fused but the inner leaflets are not. Subsequent events result in the formation of a fusion pore through which the viral contents are delivered into the cellular cytosol.

Received: January 9, 2013

Revised: April 19, 2013

Published: April 19, 2013



The transition from the hemifusion intermediate to formation of the fusion pore is thought to be the rate-limiting step in some systems.<sup>20</sup> Studies of the HIV-1 gp41 fusion peptide (analogous to the EBOV GP2 FL) and the membrane-proximal external region (MPER), a Trp-rich segment that lies between the CHR and the transmembrane (TM) domain, indicate that these segments have membrane binding activity.<sup>21–26</sup> It has been proposed that the gp41 MPER induces lipid mixing by forming a kinked  $\alpha$ -helix that embeds along the membrane surface as a result of its high tryptophan content.<sup>27,28</sup> These results suggest that the fusion peptide and MPER are involved in promoting late fusion events for HIV-1 gp41, possibly by facilitating the hemifusion to fusion pore transition.<sup>26,29</sup> Furthermore, the native MPER sequence of gp41 is required for infection and is the target of broadly neutralizing antibodies.<sup>21,27,28</sup>

In EBOV GP2, NMR structures of a peptide representing the FL at neutral and low pH revealed that it adopts an extended loop structure at pH 7 and bends 90° at pH 5.5 to adopt a membrane lytic active form.<sup>30</sup> However, the GP2 MPER has not been characterized in detail. The MPER was not included in any of three reported GP2 core domain structures in the postfusion conformation, so there is limited structural information available for this region.<sup>17–19</sup> Sáez-Cirión et al. conducted studies of a peptide representing the “pre-TM” region that contains the MPER and concluded this peptide is largely  $\alpha$ -helical and membrane-destabilizing.<sup>31</sup> However, these structural studies were largely low-resolution (infrared spectroscopy), and the behavior under low-pH conditions was not explored.<sup>32</sup>

Here we describe a detailed characterization of peptides representing the GP2 MPER. Peptides of the EBOV and SUDV MPER regions were synthesized and characterized using circular dichroism (CD), tryptophan fluorescence, and NMR in the presence of sodium dodecyl sulfate (SDS) and dodecylphosphocholine (DPC). These peptides were functionally characterized by performing viral entry inhibition assays with VSV-pseudotyped virus, vesicle leakage assays using large unilamellar vesicles (LUVs), and hemolysis assays.

## MATERIALS AND METHODS

**Materials.** *N,N*-Dimethylformamide (DMF), dichloromethane (DCM), hydroxybenzotriazole (HOBt), and 2-(1*H*-benzotriazol-1-yl)-1,1,3,3-tetramethyluronium hexafluorophosphate (HBTU) were obtained from AGTC Bioproducts (Wilmington, MA). *N,N*-Diisopropylethylamine (DIEA), acetic anhydride, trifluoroacetic acid (TFA), thioanisole, 1,2-ethanedithiol, trifluoroethanol (TFE), and 36.5–38% hydrochloric acid and sodium dodecyl sulfate (SDS) were obtained from Sigma-Aldrich (St. Louis, MO). Fmoc-protected amino acids were obtained from Applied Biosystems/Life Technologies Corp. (Carlsbad, CA) or AGTC Bioproducts. Rink Amide AM Resin (200–400 mesh) was obtained from NovaBiochem (Hohenbrunn, Germany). Acetonitrile was obtained from Fisher Scientific (Pittsburgh, PA). DPC, 1-palmitoyl-2-oleoylphosphatidylcholine (POPC), and the Liposofast Mini Extrusion system were obtained from Avanti Polar Lipids, Inc. (Alabaster, AL). GP-pseudotyped virus was obtained from K. Chandran. HyClone (Logan, UT) Dulbecco’s modified Eagle’s medium with 4 mM glutamine and 4.5 g/L glucose was used to perform the peptide inhibition assays. For the calcein leakage assays, phosphate-buffered saline (PBS) was obtained from Thermo Scientific (Amarillo, TX), and *N*-[tris-

(hydroxymethyl)methyl]-2-aminoethanesulfonic acid (TES buffer), sodium citrate, calcein, and Triton X-100 were obtained from Sigma-Aldrich. Fresh human red blood cells (hRBCs) were obtained from Research Blood Components, LLC (Brighton, MA).

**Peptide Synthesis and Purification.** Peptides were synthesized on an Applied Biosystems 433A synthesizer using the *N* $\alpha$ -Fmoc protecting group strategy. Rink amide resin (0.1 mmol) was loaded into the reaction vessel, and each Fmoc-protected amino acid was loaded into reaction cartridges at a 3-fold molar excess. The N-terminus of the peptides were acetylated using a 50% acetic anhydride/DCM mixture. Simultaneous side chain deprotection and cleavage were conducted by treatment with 95% TFA, 2.5% thioanisole, and 2.5% 1,2-ethanedithiol for 3 h. After the resin was filtered, the crude peptide was precipitated, washed twice with cold diethyl ether, and pelleted. The pellet was suspended in a water/acetonitrile mixture and then lyophilized. Crude lyophilized peptide was redissolved in a water/acetonitrile mixture and purified by reverse-phase high-performance liquid chromatography (HPLC) on a Vydac C18 column (10  $\mu$ m, 25 mm  $\times$  21.2 mm) with water/acetonitrile mobile phases containing 0.1% TFA. Purified peptide was lyophilized and redissolved in 10 mM phosphate buffer (pH 7.1). For NMR, viral entry inhibition, vesicle leakage, and hemolysis assays, the trifluoroacetate counterions were exchanged for chloride ions by dissolving the lyophilized peptide in 50 mM hydrochloric acid and lyophilizing. This process was repeated twice. The peptide purity was determined using analytical reverse-phase HPLC and estimated to be >90% in for both peptides. The peptide mass was confirmed using matrix-assisted laser desorption ionization time-of-flight (MALDI-TOF). Concentrations were determined by the absorbance at 280 nm using an extinction coefficient of 22000 M<sup>-1</sup> cm<sup>-1</sup>.

**Circular Dichroism Spectroscopy.** All spectra were acquired on a Jasco J-815 spectrometer with a 1 mm quartz cuvette. Peptides were dissolved to a concentration of 44.5  $\mu$ M in the appropriate buffer (10 mM phosphate buffer at pH 7.1 or 10 mM sodium acetate at pH 4.6). Wavelength scans were conducted in duplicate at a 0.5 nm step size and a speed of 2 nm/s from 190 to 260 nm. Background scans without peptide were also obtained and subtracted from the wavelength scans prior to converting millidegrees to mean residue ellipticity ( $\theta$ ). For the TFE experiments, a 60% TFE solution was made in the appropriate buffer. SDS titrations were performed by first obtaining a wavelength scan with peptide in the appropriate buffer without detergent; SDS was then added from a 100 mM stock solution in 0.5 mM increments from 1 to 10 mM, and the spectra were recorded. Background scans were taken independently for each concentration of SDS. DPC titrations were performed in a similar manner from a 200 mM stock solution in 0.1 mM increments from 0.1 to 2 mM. Relative CD signals in Figure 3 were calculated by obtaining  $\theta$  values at 200 and 222 nm for each concentration of SDS and DPC using the following equation: relative CD signal =  $1 - (\theta - \theta_{\text{minimum}}) / \theta_{\text{maximum}}$  (values for  $\theta_{\text{maximum}}$  and  $\theta_{\text{minimum}}$  are included in the Supporting Information).

**Tryptophan Fluorescence.** Fluorescence spectra were recorded on a Horiba Jobin Yvon fluorometer. An excitation wavelength of 295 nm was used, and the emission spectra were recorded from 300 to 450 nm with slit widths of 5 nm. For all measurements, background readings were measured for buffer alone and with the appropriate detergent concentration. For

full spectra, 1.5  $\mu$ M S-MPER was added to either 10 mM phosphate buffer at pH 7.1 or 10 mM sodium acetate at pH 4.6 with or without 20 mM SDS or DPC. DPC titrations were conducted with 1  $\mu$ M peptide in the appropriate buffer. DPC was added in 0.2 mM increments from 0.2 to 3.0 mM. SDS was added in 0.2 mM increments from 0.2 to 4.0 mM. Background was subtracted from each data set before plotting.

**NMR Spectroscopy.** NMR experiments with  $\sim$ 2 mM S-MPER peptide in 5 mM NaOAc (pH 4.6) and a  $\text{H}_2\text{O}/\text{D}_2\text{O}$  mixture (90:10) were conducted at 298 K on a Bruker Avance II instrument operating at a nominal frequency of 800 MHz equipped with a triple-resonance ( $^1\text{H}$ ,  $^{13}\text{C}$ ,  $^{15}\text{N}$ ) cryogenic probe including Z-axis pulse field gradients. Sequence specific assignments were obtained from two-dimensional (2D)  $^1\text{H}$ – $^1\text{H}$  TOCSY (15 and 80 ms mixing times), 2D  $^1\text{H}$ – $^1\text{H}$  NOESY (400 ms mixing time), 2D  $^1\text{H}$ – $^{13}\text{C}$  aliphatic HSQC, 2D  $^1\text{H}$ – $^{13}\text{C}$  aromatic HSQC, and 2D  $^1\text{H}$ – $^{15}\text{N}$  HSQC spectra. For the S-MPER peptide in 200 mM [ $^2\text{H}$ ]DPC and 5 mM NaOAc (pH 4.6), NMR experiments were conducted at 310 K on a Bruker Avance II instrument operating at a nominal frequency of 900 MHz equipped with a triple-resonance cryogenic probe. Sequence specific assignments were obtained from 2D  $^1\text{H}$ – $^1\text{H}$  TOCSY (15 and 80 ms mixing times), 2D  $^1\text{H}$ – $^1\text{H}$  NOESY (100 and 400 ms mixing times), 2D  $^1\text{H}$ – $^{13}\text{C}$  aromatic HSQC, and 2D  $^1\text{H}$ – $^{15}\text{N}$  HSQC spectra in 90%  $\text{H}_2\text{O}$  and a 2D  $^1\text{H}$ – $^{13}\text{C}$  aliphatic HSQC spectrum in 100%  $\text{D}_2\text{O}$ . The 2D  $^1\text{H}$ – $^1\text{H}$  TOCSY/NOESY spectra were acquired with Excitation Sculpting water suppression.<sup>33</sup> For the 5-doxyl stearate experiments, a stock solution of the paramagnetic agent was dissolved in a  $\text{CHCl}_3$ /methanol mixture (2:1); the correct amount for a concentration of 6 or 9 mM was transferred to an Eppendorf tube and dried under argon gas, and the peptide, previously dissolved in 200 mM DPC micelles (100%  $\text{D}_2\text{O}$ ), was added. 2D  $^1\text{H}$ – $^{13}\text{C}$  aliphatic and  $^1\text{H}$ – $^{13}\text{C}$  aromatic HSQC spectra were recorded on a Varian Inova 600 MHz spectrometer equipped with a triple-resonance cryoprobe at 310 K. All of the  $^1\text{H}$ – $^{13}\text{C}/^{15}\text{N}$  HSQC spectra were recorded as nonuniform sampled experiments (50% sampling) and processed using the Compressed Sensing algorithm in MDDNMR version 2.1.<sup>34</sup> All spectra were processed using NMRpipe/NMRDraw<sup>35</sup> and the data analyzed using CCPN Analysis.<sup>36</sup> Secondary chemical shifts for  $^{13}\text{C}\alpha$  and  $^{13}\text{C}\beta$  chemical shifts were calculated from the difference method between measured values and random-coil values of  $^{13}\text{C}\alpha$  and  $^{13}\text{C}\beta$ .<sup>37</sup> Chemical shifts were referenced to DSS in the samples.<sup>38</sup> The secondary structure propensity (SSP) scores were calculated using the SSP program<sup>39</sup> using  $^1\text{H}\alpha$ ,  $^{13}\text{C}\alpha$ , and  $^{13}\text{C}\beta$  chemical shifts. Average chemical shift changes for the backbone amide  $^1\text{H}$  and  $^{15}\text{N}$  nuclei ( $\Delta\delta_{\text{av}}$ ) of the S-MPER peptide were calculated using the relationship  $\Delta\delta_{\text{av}} = \{[(\Delta\delta\text{H})^2 + 0.2(\Delta\delta\text{N})^2]/2\}^{1/2}$ , where  $\Delta\delta\text{N}$  represents the change in the amide nitrogen chemical shift and  $\Delta\delta\text{H}$  represents the change in the amide chemical shift.<sup>40</sup>

**Peptide Entry Inhibition Assays.** Entry assays were performed essentially as described previously.<sup>41</sup> Vero cells ( $7.5 \times 10^4$  cells) were plated in a 48-well plate in the presence of 2% (v/v) FBS and 1% (v/v) Pen-Strep the day prior to experiments, resulting in cell confluency the following day. Peptide was added to the appropriate wells. After preincubation for 1 h with peptides, GP-pseudotyped virus was added to the wells and incubated for an additional 1 h. Infection was stopped with 20  $\mu$ M ammonium chloride to neutralize endosomal pH,

and infection was scored the following day by manually counting eGFP-positive cells under a fluorescence microscope.

**Leakage from Large Unilamellar Vesicles.** POPC LUVs were generated by making a chloroform solution containing 152 mg of POPC, drying under reduced pressure to form a thin film, and mixing with a 2 mL solution of 10 mM TES, 100 mM sodium citrate, and 40 mM calcein. Following 20 freeze–thaw cycles, the liposome suspension was extruded through a 100 nm polycarbonate membrane (Whatman Nuclepore Track-Etch Membrane) 21 times as required, at room temperature. Gel filtration (ÄKTA FPLC with a HiPrep 16/60 Sephacryl TM-S-500HR column) was used to remove any free calcein. The lipid concentration was determined by a Stewart assay,<sup>42</sup> and the liposome size was confirmed by dynamic light scattering (DLS) on a DynaPro nanostar (Wyatt, Santa Barbara, CA). DLS showed a hydrodynamic diameter of 100 nm and a polydispersity in the range of 15–30%. The instrument setup used standard PBS parameters; the refractive index was 1.333 (589 nm, 20 °C), the viscosity 1.019 cP, and the Cauchy coefficient 3119 nm<sup>2</sup>. Data were acquired in autoattenuation mode and processed with DYNAMIC V6TM.

The calcein leakage assay was performed by incubating 100  $\mu$ M S-MPER (obtained by dilution from a 1.4 mM peptide stock solution) with 500  $\mu$ M LUVs for 30 min, at pH 7 and 4.6. Leakage was assessed by measuring calcein fluorescence ( $I$ ) at 520 nm ( $\lambda_{\text{ex}} = 485$  nm) on a fluorescence spectrometer (Horiba Jobin Yvon Fluorolog FL 3-22). At the end of the experiments, the LUVs were lysed completely with Triton X-100 [1% (w/v)]. The percent leakage was calculated using the expression  $(I - I_0)/(I_{\text{total}} - I_0) \times 100$ , where  $I_0$  is the fluorescence intensity before the addition of the peptide and  $I_{\text{total}}$  is the fluorescence intensity after the addition of Triton X-100. Leakage experiments using the fY-magainin 2 peptide were performed in a similar manner, as described in ref 41. Each experiment was repeated twice, independently. Data reflect the average of the two sets of experiments.

**Hemolysis Assays.** For the hemolytic assay, fresh hRBCs were centrifuged at 3500 rpm and washed with PBS until the supernatant was clear. The hRBCs were resuspended and diluted to a final concentration of 1% (v/v) in PBS (pH 7.4 or 4.6) and used immediately. The PBS for this assay consisted of 0.14 M NaCl, 2.7 mM KCl, 10.1 mM  $\text{Na}_2\text{HPO}_4$ , and 1.76 mM  $\text{KH}_2\text{PO}_4$  (pH 7.4) in deionized water. To perform the assay, 5  $\mu$ L of several dilutions of S-MPER in PBS, or PBS alone, was added to 500  $\mu$ L of hRBCs in PBS, gently shaken, and incubated at 37 °C for 1 h. The incubated mixture was centrifuged at 3500 rpm for 10 min, and the supernatant was diluted 1:1 (v/v) in water (50  $\mu$ L each) in a clear bottom sterile 96-well plate. Release of hemoglobin was monitored at 415 nm using a plate reader. To calculate the percentage of hemolysis, we used the expression  $(A_{415,\text{peptide}} - A_{415,\text{buffer}})/(A_{415,\text{complete hemolysis}} - A_{415,\text{buffer}})$ , where complete hemolysis was determined by mixing hRBCs with 1% Triton X-100. The experiment was also performed with the positive control Gramicidin A, essentially as described previously.<sup>44</sup> Each condition was used in triplicate, and the standard deviation was calculated for each data point.

## RESULTS

**Design and Synthesis of EBOV MPER Peptides.** The MPER of class I fusion proteins is defined as the tryptophan-rich region between the CHR and the TM of the trans-membrane subunit. Crystallographic and limited proteolysis

studies indicate the CHR  $\alpha$ -helix ends at or around Asp632 for EBOV GP2, and in fact, the sequence falls out of the canonical heptad repeat at this point.<sup>17–19</sup> The TM is predicted by hydropathy analysis to begin at position ~658 for EBOV GP2.<sup>31</sup> As shown in Figure 1, the region from Asp632 to

EBOV:	632-DKTLPPDQGDNDNWWTGWRQW-651
BDBV:	632-DKPLPDQTDNDNWWTGWRQW-651
SUDV:	632-DNPLPNQDNDNWWTGWRQW-651
TAFV:	632-DNNLPNNDGSDNWWTGWRQW-651
RESTV:	633-DNPLPDHGDDLNLWTGWRQW-652
FIV:	767-LQKWEDWVGWIGNIPQYLKG-786
HIV-1:	660-LLELDKWSLWNWFDITNWLWYIK-683

**Figure 1.** Amino acid alignment of GP2 MPER regions from type members of the five species of genus *Ebolavirus* (BDBV, Bundbugyo virus; TAFV, Thai Forest virus). Residues that are identical in at least four of the viruses are highlighted in gray (hydrophobic) or boxed (polar). For comparison, the MPER segments of FIV and HIV-1 gp41 are included. Z-MPER and S-MPER peptides correspond to the sequences shown here for EBOV and SUDV, respectively. N- and C-termini of peptides were blocked with acetyl and amide groups, respectively.

Trp651 (EBOV numbering) contains a high tryptophan content, particularly in the Trp644–Trp651 segment, and therefore, we focused on this segment. This region is well conserved among the five species within the genus *Ebolavirus* (Figure 1; note that for the type member of the species *Reston Ebolavirus*, this segment corresponds to residues Asp633–Trp652). There are four conserved tryptophans at positions 644, 645, 648, and 651 (EBOV numbering). There is a proline residue near the N-terminus that may result in conformational constraints in this region.<sup>45</sup> There are several other conserved residues with a range of physicochemical properties, all likely to contribute to the overall structure and function of this region. In particular, residues 643–651 of GP proteins derived from members of all *Ebolavirus* species, but one sequence (RESTV) is completely conserved; notably, RESTV is not pathogenic in humans. Moreover, some positions are conserved with respect to charge; for example, residue 650 varies between arginine and lysine. The degree of conservation and high tryptophan content suggest that the Ebola virus MPER has membrane binding or perturbing activity and is likely analogous to the HIV-1 MPER even though these two viruses are evolutionarily distinct.

The EBOV and SUDV MPER were chosen for this study because they are the most prevalent and pathogenic among the ebolaviruses. Peptides corresponding to these regions (Z-MPER for EBOV and S-MPER for SUDV) were produced using solid-phase peptide synthesis with the standard Fmoc protecting group strategy. The N-termini were blocked with an acetyl group and the C-termini by an amide. Deprotection/cleavage and purification by RP-HPLC followed standard protocols. The identity of the purified peptides was verified by MALDI-TOF, and the purity was judged to be >90% by analytical RP-HPLC (see the Supporting Information).

**Effects of Cosolvents and Detergents Assessed by Circular Dichroism (CD) Spectroscopy.** CD spectroscopy was used to assess the overall secondary structure of Z-MPER and S-MPER. The FL undergoes a conformational change at endosomal pH to a form that induces rapid lipid mixing.<sup>30</sup> It is reasonable to predict that the MPER also forms a membrane-active conformation at endosomal pH that differs from its conformation at neutral pH. Therefore, CD spectra were

recorded at pH 7.1 in 10 mM phosphate buffer (PB) and pH 4.6 in 10 mM sodium acetate (NaOAc) buffer to represent the conditions at the plasma membrane and endosomal membrane, respectively (Figure 2A). The CD signatures of both peptides had a pronounced minimum at 200 nm and a slight shoulder at 220 nm, but no other minima or maxima under either pH condition. These CD spectra are indicative of a mixed or slightly helical conformation, although the curve shape may be obscured to some extent by far-UV interference from the tryptophans of the peptides. However, the near-UV spectrum did not appear to have any rotational properties (data not shown).

To assess the structural properties of Z-MPER and S-MPER in the presence of a structure-promoting cosolvent, CD spectra were recorded at pH 7.1 and 4.6 in the presence of 60% (v/v) trifluoroethanol (TFE) (Figure 2A). It is believed that TFE induces secondary structure in short peptides by promoting intramolecular hydrogen bonding.<sup>46</sup> The CD spectra of Z-MPER and S-MPER in 60% TFE resulted in a slightly right-shifted minimum (to 201 nm) and the formation of a second minimum near 217 nm. Although these spectra do not reflect a specific secondary structure, the tendency toward a double minimum suggests that these peptides have helical propensities.

To determine whether Z-MPER and S-MPER interact with lipids, titrations with SDS and DPC were performed at pH 7.1 and 4.6. SDS forms negatively charged micelles at a critical micelle concentration (CMC) of 8.3 mM, and DPC forms zwitterionic micelles at a CMC of 1.1 mM.<sup>47,48</sup> Titrations of S-MPER with up to 10 mM SDS resulted in a lipid-dependent change in the CD spectrum at both pH values, reflected by the formation of a double minimum (Figure 2B,C). Overall, there was a gradual decrease in the amplitude of the 200 nm minimum with an increasing SDS concentration and a simultaneous gradual appearance of a 222 nm minimum, eliminating the original 220 nm shoulder. An overlay of spectra recorded at various SDS concentrations revealed an isodichroic point at ~218 nm, suggesting the change in the CD spectrum reflects a two-state conformational transition. Similar results were obtained upon titration of Z-MPER with SDS (Figure 2F,G).

Titration with up to 2 mM DPC resulted in a similar change to the CD spectra for both S-MPER and Z-MPER under both pH conditions (Figure 2D,E,H,I). For both peptides, a minimum at 222 nm developed with increasing amounts of DPC and the amplitude of the minimum at ~200 nm decreased; an isodichroic point was observed at ~215 nm. However, the ratios of the signal intensities for these two minima at high DPC concentrations contrasted with the signal ratios at high SDS concentrations; with 2 mM DPC, the 200 nm band was more intense than the 222 nm band, whereas the opposite relative ratio of the 200 and 222 nm bands was observed in 10 mM SDS. In addition, an increasing DPC concentration resulted in the appearance of a positive band at 233 nm; this positive band was not observed with increasing SDS concentrations.

When the normalized CD signals at 200 and 222 nm were plotted as a function of peptide:lipid concentration ratio ([P]:[L]), the conformational transition, defined by the intersection of the 200 and 222 nm plots, occurs at [P]:[L] values of  $1.5 \times 10^{-2}$  (3.3 mM SDS) at pH 7.1 and  $2.5 \times 10^{-2}$  (1.8 mM SDS) at pH 4.6 for S-MPER [44.5  $\mu$ M peptide (Figure 3A)]. Interestingly, these transitions occurred at SDS concentrations below the CMC under standard conditions (8.3 mM). Z-

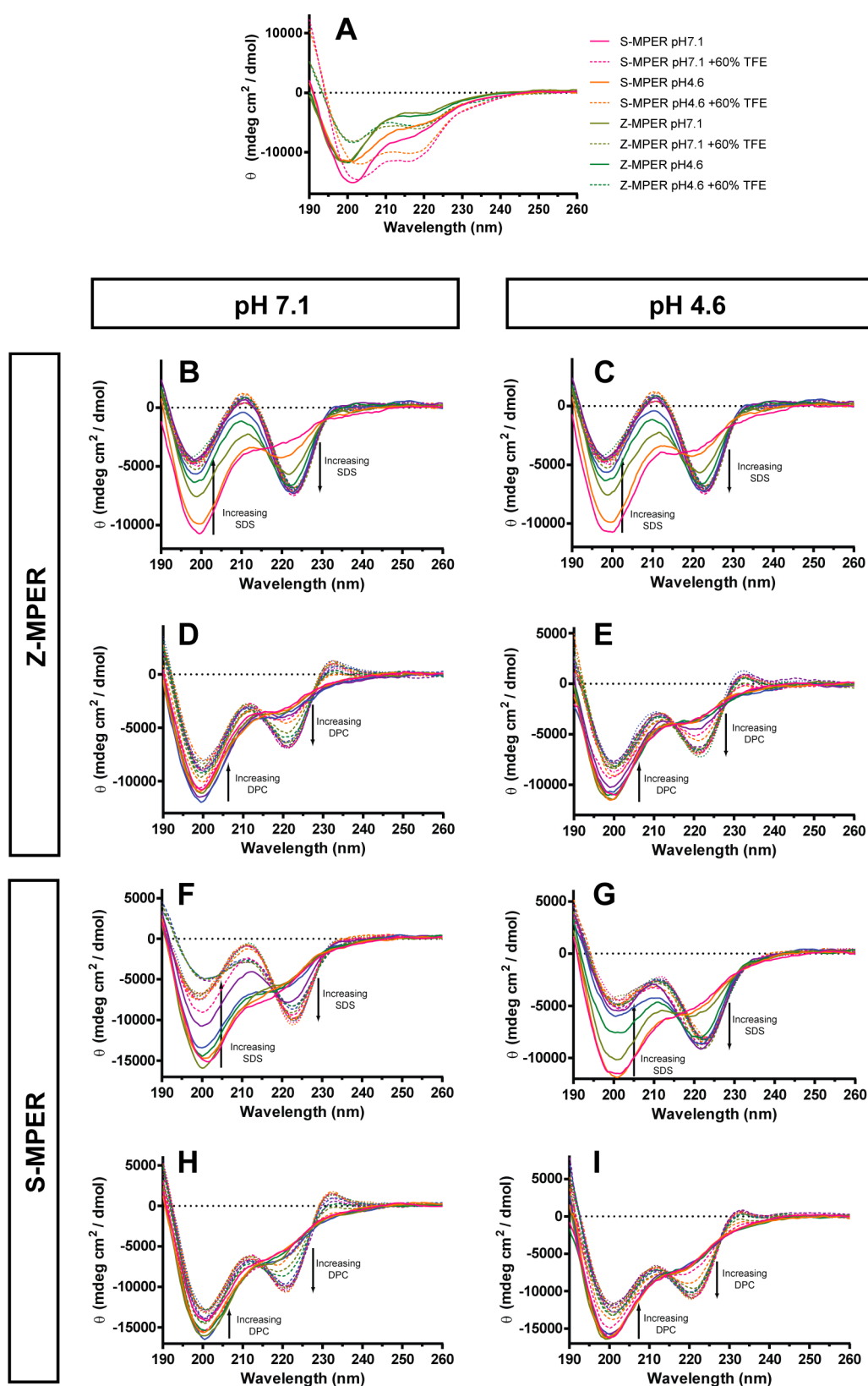


**Figure 2.** CD spectra of Z-MPER and S-MPER under various conditions. (A) Peptides with or without 60% TFE. (B–E) Z-MPER titrations with SDS (B and C) or DPC (D and E) pH 4.6 and 7.1. Data were acquired at SDS concentrations of up to 10 mM in 0.5 mM increments and at DPC concentrations of up to 2 mM in 0.1 mM increments. (F–I) Similar analysis of S-MPER.

MPER was also affected by pH (experiments performed at identical peptide concentrations), undergoing an apparent conformational change at  $[P]:[L]$  values of  $2.6 \times 10^{-2}$  (1.7

mM SDS) at pH 7.1 and  $3.7 \times 10^{-2}$  (1.2 mM SDS) at pH 4.6 (Figure 3B). Because SDS titration experiments for both S-MPER and Z-MPER were performed at identical peptide

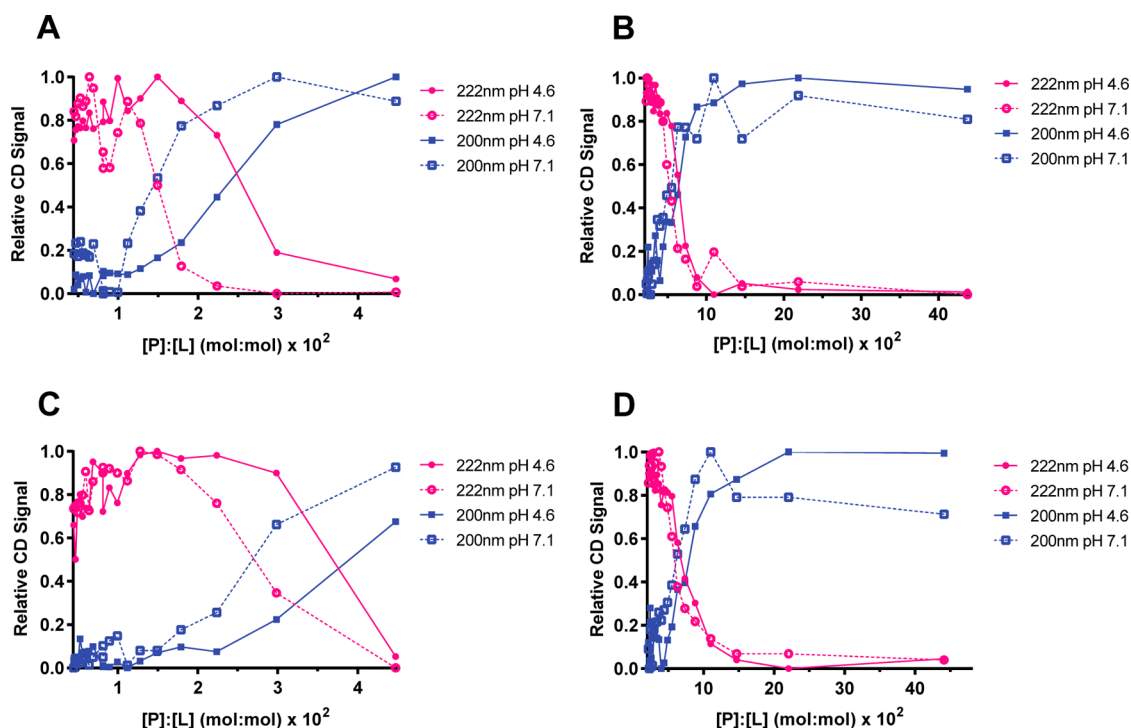


**Figure 3.** CD signal at 200 and 222 nm as a function of  $[P]:[L]$ . Relative CD signals were calculated by  $\theta$  values at 200 and 222 nm for each concentration of SDS and/or DPC using the following equation: relative CD signal =  $1 - (\theta - \theta_{\text{minimum}})/\theta_{\text{maximum}}$ . (A) S-MPER with SDS. (B) S-MPER with DPC. (C) Z-MPER with SDS. (D) Z-MPER with DPC.

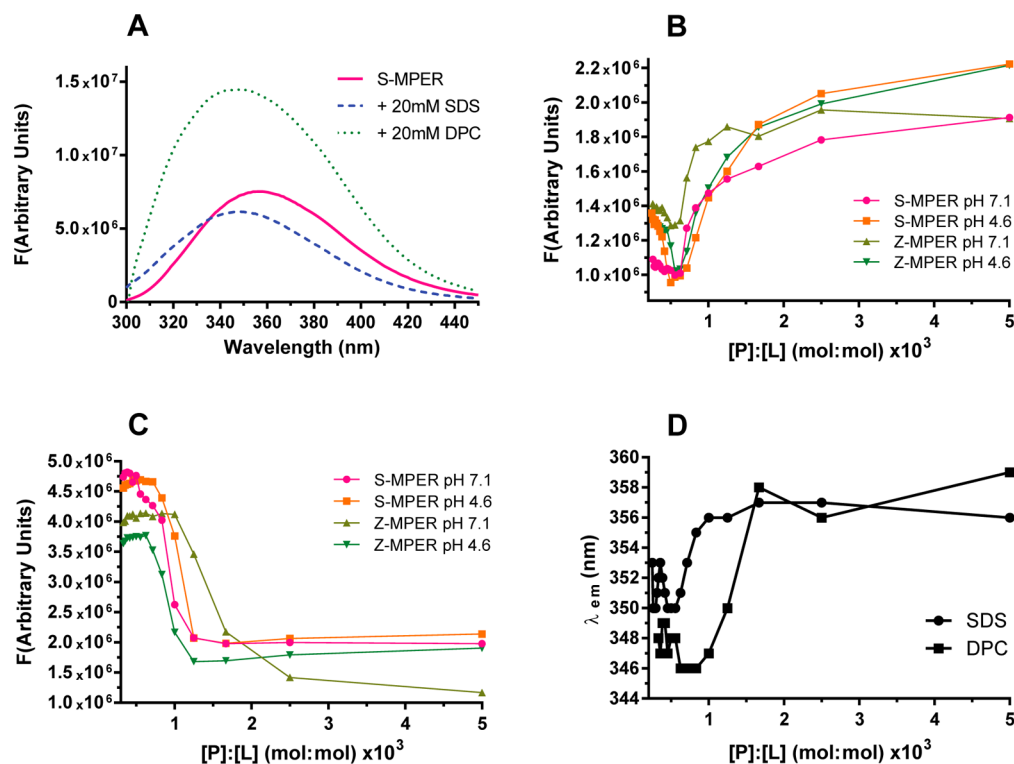


**Figure 4.** Effects of micelle-forming detergents on tryptophan fluorescence. (A) Emission spectra of S-MPER alone and in the presence of 20 mM SDS or 20 mM DPC. (B and C) Effects of SDS (B) or DPC (C) on emission at 354 nm. (D) Change in emission maximum ( $\lambda_{\text{em}}$ ) upon detergent binding for S-MPER.

concentrations, it is likely that the observed differences in  $[P]:[L]$  at which the conformational transition occurs reflect innate differences in how the two peptides interact with SDS micelles. The sequences of S-MPER and Z-MPER differ in their

predicted charges at neutral pH ( $-3$  for S-MPER and  $-2$  for Z-MPER) and in the overall pattern of negatively charged residues (Asp) in the N-terminal half. Because SDS micelles contain anionic headgroups, it is reasonable to expect that lipid

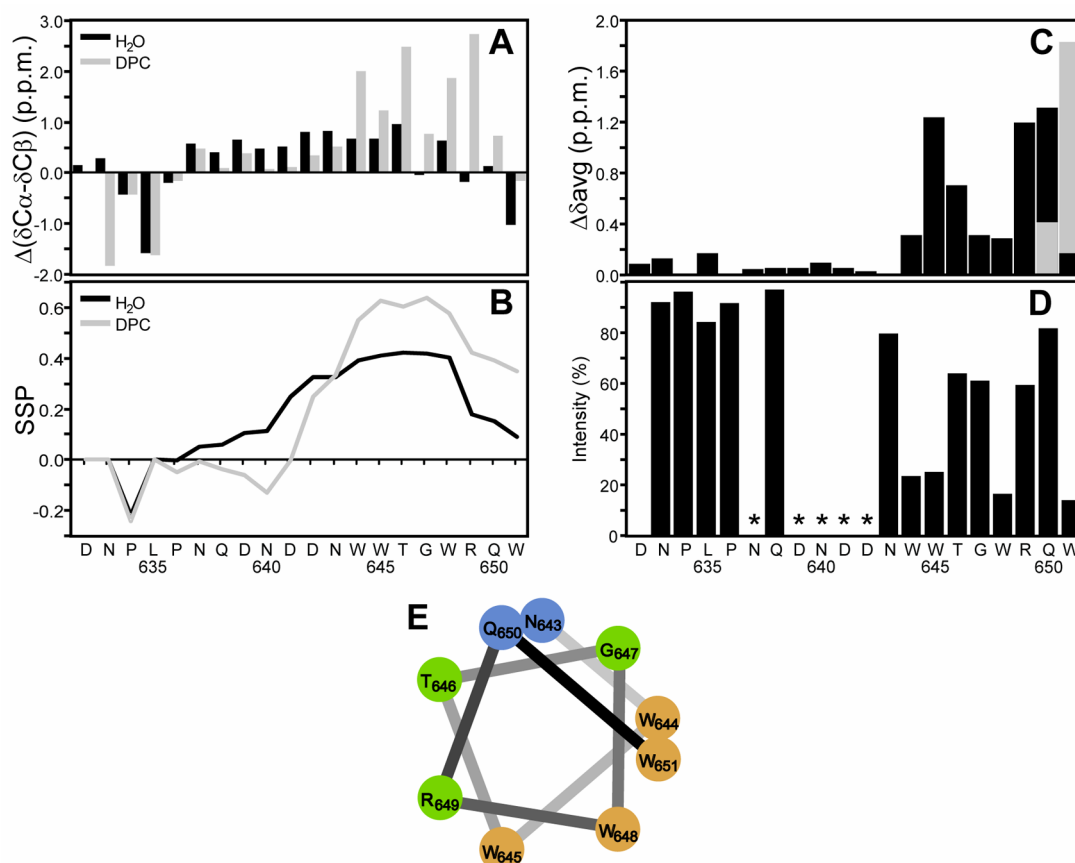


**Figure 5.** Nuclear magnetic resonance of S-MPER. (A) Chemical shift deviations from random coil shifts for  $\delta C\alpha$  and  $\delta C\beta$ . (B) Secondary structure propensity (SSP) scores for S-MPER in  $H_2O$  (black) and 200 mM DPC micelles (gray) calculated using  $^{13}C\alpha$ ,  $^{13}C\beta$ , and  $^1H\alpha$  chemical shifts. Positive values represent helical propensity. (C) Average amide chemical shift differences,  $\{[(\Delta\delta^1H)^2 + 0.2(\Delta\delta^{15}N)^2]/2\}^{1/2}$ , for S-MPER in  $H_2O$  vs 200 mM DPC micelles. The alternative chemical shift difference for the ambiguous assignment of the amide correlations of Q19/W20 is colored gray. (D) Effect of a paramagnetic agent on S-MPER in 200 mM DPC micelles in  $D_2O$  for the correlation of the last protonated carbon of each amino acid in the aliphatic  $^1H$ - $^{13}C$  HSQC spectrum (except that the  $C\gamma$ - $H\gamma$  and  $H$ - $C3\epsilon$  correlations were used for Pro and Trp). The ratio of integrated cross-peak intensities with and without 9 mM 5-doxyl stearate is plotted along with the amino acid sequence. Residues for which it was not possible to obtain reliable intensity ratios because of overlapping cross-peaks are marked with asterisks. (E)  $\alpha$ -Helical wheel representation of the C-terminal residues (12–20) of S-MPER color-coded by percent intensity loss upon addition of 9 mM 5-doxyl stearate: brown for >50%, green for 35–50%, and blue for <35%.

binding (and therefore conformational transition) would occur at lower  $[P]:[L]$  values for Z-MPER because it has less overall charge. Furthermore, the  $[P]:[L]$  value at which the conformational transition takes place appears to be pH-sensitive (occurring at lower  $[P]:[L]$  values at pH 7.1 than at pH 4.6 for both peptides). This pH dependence may reflect intrinsic conformational tendencies of the peptides in the context of anionic lipids. Alternatively, this behavior may result from differences in SDS micelle formation at different concentrations (the CMC for SDS is pH-dependent, with a lower CMC at a lower pH). These two possibilities are not mutually exclusive, and therefore, these effects may also be due to some combination of the two.

Differences in behavior between the two peptides and at the two pH values were less pronounced in titrations with DPC (Figure 3B,D). A conformational transition took place at  $[P]:[L]$  values of  $6.0 \times 10^{-2}$  (0.7 mM DPC) at pH 4.6 and  $5.0 \times 10^{-2}$  (0.8 mM DPC) at pH 7.1 for S-MPER. For Z-MPER, these conformational changes took place at  $[P]:[L]$  values of  $7.4 \times 10^{-2}$  (0.6 mM DPC) and  $6.0 \times 10^{-2}$  (0.7 mM DPC) at pH 4.6 and 7.1, respectively.

The CD signatures observed in the presence of high SDS and DPC concentrations do not match those of any of the canonical secondary structures, likely because of interference by tryptophan in a manner that is dependent on membrane context. Therefore, the spectra in Figure 2B–I do not provide direct secondary structural information. Nonetheless, it can be concluded that there is a conformational transition in these peptides upon addition of micelle-forming surfactants SDS and DPC. TFE appears to have some effect on the CD signature, in a manner that is distinct from effects observed in SDS or DPC.

**Tryptophan Fluorescence Studies.** The Trp-rich content of the GP2 MPER permits the use of Trp fluorescence to detect binding of S-MPER and Z-MPER to SDS and DPC micelles. The typical emission maximal wavelength ( $\lambda_{em}$ ) of Trp-containing peptides is 354 nm in aqueous solution and shifts toward lower wavelengths in apolar environments.<sup>24–26,49</sup> Addition of 20 mM SDS or DPC to S-MPER at pH 7 resulted in a blue shift in  $\lambda_{em}$  from 354 to 347 nm (Figure 4A; emission spectra were obtained via excitation at 295 nm). A large increase in fluorescence intensity resulted upon addition of DPC, a phenomenon that is commonly observed when Trp-rich peptides interact with lipids containing a positive charge.<sup>50</sup>

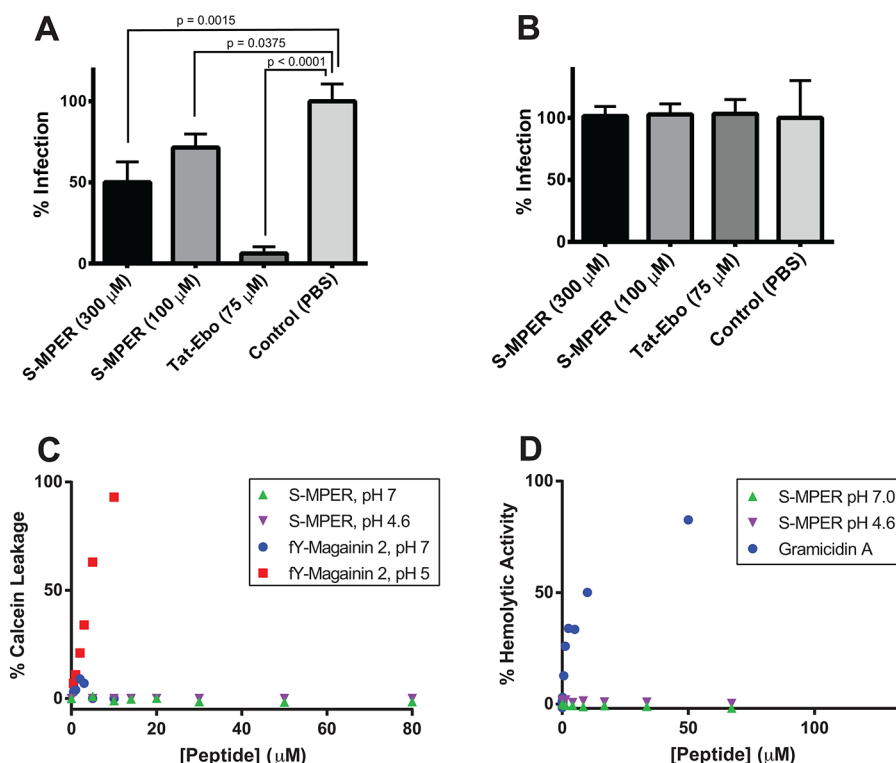


**Figure 6.** Biological and membrane perturbing assays with S-MPER. (A) Inhibition of VSV-GP entry by S-MPER. The potent entry inhibitor Tat-Ebo (ref 41) was used as a positive control. (B) Control entry assay using VSV-G. (C) Leakage assays with 500  $\mu$ M POPC LUVs. Experiments were performed twice independently with similar results; a representative data set is shown. (D) Hemolysis assays.

A decrease in fluorescence intensity typically occurs when tryptophans interact with lipids containing a negatively charged headgroup; this effect was observed upon addition of SDS to S-MPER. Similar results were obtained with Z-MPER (data not shown). Taken together, the changes in fluorescence intensity and the blue shift of  $\lambda_{em}$  are indicative of an interaction between S-MPER and the lipid headgroups of SDS and DPC.

Titration of S-MPER and Z-MPER with SDS and DPC were conducted at pH 7.1 and 4.6 to determine the [P]:[L] at which the binding interaction occurs. Titration of both peptides with SDS showed a decrease in the fluorescence intensity at a low [P]:[L] ( $<0.5 \times 10^{-3}$ ), followed by an increase to a maximum with a transition at a [P]:[L] of  $\sim 0.7 \times 10^{-3}$ . There were minor differences among the two peptides and pH conditions, but the overall trends were similar. This contrasts with the behavior observed by CD, where there were differences in [P]:[L] at which transition occurred for the various peptides and pH conditions. Furthermore, the specific [P]:[L] at which binding was observed did not correlate with the transition observed by CD. These discrepancies could be a consequence of the fact that the fluorescence experiments were conducted at a much lower peptide concentration (1  $\mu$ M vs 44.5  $\mu$ M for the CD studies). The initial decrease in fluorescence intensity is not correlated with the characteristic blue shift in  $\lambda_{em}$  (Figure 4D shows a plot of  $\lambda_{em}$  vs [P]:[L] for S-MPER), but the larger transition at a [P]:[L] of  $\sim 0.7 \times 10^{-3}$  is correlated with the blue shift. Therefore, we conclude that the transition represents the binding event and effects at lower [P]:[L] values may be due to other effects.

Titration of both peptides with DPC resulted in a sigmoidal decrease in fluorescence intensity that was coupled with a blue shift (Figure 4D). The transition for both peptides occurred at [P]:[L] values of  $0.6 \times 10^{-3}$  (0.7 mM DPC) at pH 7.1 and 0.8

$\times 10^{-3}$  (0.9 mM DPC) at pH 4.6. The behaviors of both S-MPER and Z-MPER were similar to one another and similar across both pH conditions, consistent with the CD observations.

Together, results from these studies suggest that the GP2 MPER sequences have the potential to bind and insert into surfactant micelles, and that this binding event is correlated with a conformational transition in the MPER peptides. The behavior of the peptides as monitored by fluorescence and CD for binding to DPC was consistent, indicating that the binding and conformational transition is not dependent on pH and that peptides from the two species had similar activity. The titration of peptides with SDS yielded less straightforward results when monitored by fluorescence and did not correlate precisely with effects observed by CD. These results may reflect the fact the SDS is anionic while DPC is zwitterionic and therefore closer to the native mammalian or viral membranes.

**Nuclear Magnetic Resonance (NMR) Analysis of S-MPER Structure and Detergent Interactions.** NMR spectroscopy was used to obtain more detailed, sequence specific information about the secondary structure of the S-MPER peptide and its interaction with micelles. Essentially complete  $^1\text{H}$ ,  $^{13}\text{C}$ , and  $^{15}\text{N}$  resonance assignments for both the peptide alone (Table S1 of the Supporting Information) and the peptide in the presence of 200 mM deuterated DPC (Table S2 of the Supporting Information) were made using 2D TOCSY and NOESY spectra for sequential  $^1\text{H}$  assignments, with natural abundance  $^1\text{H}$ - $^{13}\text{C}$  and  $^1\text{H}$ - $^{15}\text{N}$  HSQC spectra being used to obtain the corresponding  $^{13}\text{C}$  and  $^{15}\text{N}$  chemical shifts (Figures S1–S3 of the Supporting Information, respectively). In the absence of detergent, the peptide appeared to be essentially unstructured, with no NOEs indicative of secondary structure observed. Most backbone chemical shifts

were near their random coil values, although they were slightly shifted toward helical values for Asn637–Gly647 (Figure 5A), leading to a 10–40% helical propensity (Figure 5B) as defined by secondary structure propensity (SSP) chemical shift analysis.<sup>39</sup> Upon addition of 200 mM DPC, there were only small chemical shift changes for N-terminal residues Asp632–Pro636, a slight decrease from the helical shifts in residues Trp644 and Asn643, and a significant increase toward helical secondary shifts for C-terminal residues Trp644–Gln650 (Figure 5A), leading to a loss of helical propensity for residues 637–642, and an increased helical propensity of up to 60% from Trp644 onward. Only a few readily identifiable backbone NOEs consistent with helical structure were observed; this is partly due to the limited chemical dispersion in the spectrum of this fairly repetitive sequence, but mainly a result of the peptide not forming a stable, fully structured conformation even in the presence of DPC.

Significant detergent-induced chemical shift changes were observed for the backbone amide <sup>1</sup>H–<sup>15</sup>N resonances of the C-terminal segment of S-MPER (Figure 5C), consistent with only those residues (Trp644–Trp651) interacting with the detergent micelle. Because these changes could result from interactions with detergent micelles, conformational changes, or a combination of the two, the lipophilic paramagnetic broadening agent 5-doxyl stearate was used as a direct probe of membrane interactions. The doxyl nitroxide group at C5 of the C18 stearic acid is a moderately shallow depth probe that broadens and reduces the intensity of NMR cross-peaks from groups on the surface and partially inserted into the detergent micelle in which it is incorporated. As shown in Figure 5D, the side chain resonances of the first 12 residues of S-MPER were unaffected by incorporation of 9 mM doxyl stearate into the DPC micelle. Residues Trp644–Trp651, however, showed significant decreases in intensity. These intensity changes varied with a periodicity of ~3, with the four Trp (644, 645, 648, and 651) side chains showing the largest effects. Mapping these paramagnetic relaxation effects onto a helical wheel representation of the C-terminal half of the peptide (Figure 5E) shows that the data are most consistent with a generally helical conformation for this segment, with the face of the nascent helix that contains all four Trp residues forming the surface that interacts only shallowly with the detergent micelle.

**Biological and Membrane Perturbing Assays.** The MPER segments of HIV-1 and feline immunodeficiency virus (FIV) have antiviral activity, likely because of their membrane lytic or membrane binding activity.<sup>51,52</sup> We tested the potential of S-MPER to inhibit GP-mediated cell entry using a vesicular stomatitis virus pseudotyped to display SUDV GP on its surface in place of the native G protein (“VSV-GP”). A broadly inhibiting Ebola virus C-peptide (“Tat-Ebo”) was used as a positive control.<sup>41</sup> S-MPER was found to inhibit infection by ~45% at 300  $\mu$ M and ~25% at 100  $\mu$ M (Figure 6A), with no toxic effect to the cells at these concentrations. This inhibition was specific for the envelope glycoprotein of SUDV; the peptide had no activity against VSV containing its native envelope glycoprotein G (“VSV-G”) (Figure 6B).

The ability of S-MPER to induce leakage of a self-quenching small molecule dye (calcein) from LUVs comprised of POPC was examined. As shown in Figure 6C, S-MPER did not induce leakage at either pH 4.6 or 7.0 at up to 80  $\mu$ M peptide (corresponding to a [P]:[L] of 0.16; the LUV concentration was 500  $\mu$ M). A pH-sensitive variant of magainin 2 containing trifluorotyrosine (fY-magainin 2) was used as a control; as

previously reported, fY-magainin 2 induced LUV leakage at pH 4.6 but not at pH 7.0.<sup>43</sup> However, Trp fluorescence experiments indicated that both S-MPER and fY-magainin 2 bound LUVs to a similar degree at 10  $\mu$ M peptide and pH 5.0 (Supporting Information). These results indicate that, while the S-MPER peptide is able to bind and insert into membranes, this effect does not induce leakage. These results are also consistent with the lack of cellular toxicity at a high peptide concentration (300  $\mu$ M). To further explore potential membrane lytic effects in the context of a more complex membrane system, hemolysis assays were performed with S-MPER and the peptide gramicidin A, which induces hemolysis at high concentrations, as a control (Figure 6D).<sup>44</sup> The S-MPER peptide did not have hemolytic properties at peptide concentrations of up to 140  $\mu$ M.

## DISCUSSION

The studies performed on peptides representing the MPER of EBOV and SUDV yielded three overall conclusions. (1) As a peptide, the GP2 MPER binds to micelle-forming surfactants in a pH-independent manner with a higher affinity for zwitterionic micelles. (2) A large conformational change to a more predominantly helical state occurs for the tryptophan-rich region of this peptide upon micelle binding. (3) These peptides have modest viral entry inhibitory activity but do not induce leakage from LUVs.

The CD spectra of S-MPER and Z-MPER were difficult to interpret because they did not correspond to a signature for a specific secondary structure. CD signatures of unstructured peptides typically exhibit a minimum at 195 nm and, in some cases, a positive band at 212 nm. An  $\alpha$ -helical secondary structure is characterized by a double minimum at 208 and 222 nm. The CD spectra of S-MPER and Z-MPER did not fit either of these signatures. Instead, the peptides in aqueous solution had a minimum at 200 nm and a shoulder at 220 nm and formed double minima at 200 and 222 nm in the presence of a surfactant. Aromatic residues, particularly Trp, often result in far-UV interference in CD spectra because they have fully allowed  $\pi \rightarrow \pi^*$  transitions, typically at ~220 nm. Trp-rich peptides can therefore exhibit unusual CD signatures. Furthermore, the orientation of the tryptophan indole group affects the rotational direction and ellipticity of peptides.<sup>53</sup> The high Trp content of Z-MPER and S-MPER is likely the cause of such unusual spectra.

Nonetheless, titrations of both MPER peptides with SDS and DPC revealed a conformational transition in the presence of micelle-forming surfactants, which was corroborated by the tryptophan fluorescence experiments that showed binding. Both surfactants induced a blue shift in  $\lambda_{em}$  from 354 to 346 nm indicating burial of the Trp residues in the surface of the micelles. The fluorescence intensities observed in Figure 3A are typical for binding of SDS and DPC by Trp-rich peptides. Binding to DPC results in an increase in fluorescence intensity because the positive charge of the DPC headgroup destabilizes the charge transfer energy between the Trp indole group and its amide backbone that typically acts as the electron acceptor. The opposite is true for SDS, resulting in a decrease in fluorescence intensity.<sup>50</sup>

The combination of CD and Trp fluorescence experiments led to two other conclusions. First, the affinity of the interaction of Z-MPER and S-MPER with DPC micelles is higher than the affinity of that with SDS. When the interactions with SDS are analyzed, the shape of the fluorescence titration curves (Figure

4C) and the apparent pH-dependent conformational transition in the CD studies (Figure 3A,B) indicate that the peptides interact with SDS in a manner distinct from that of DPC. Hence, Z-MPER and S-MPER interact specifically with physiologically relevant zwitterionic membranes. The second conclusion drawn from these experiments was that Z-MPER and S-MPER appear to interact with DPC in a pH-independent manner. This finding contrasts with the reported behavior of the FL, which undergoes a pH-dependent conformational change to a membrane-active form that is competent for inducing lipid mixing.<sup>30</sup>

Although there are slight differences in the [P]:[L] at which conformational transitions occur in DPC, this is likely due to subtle changes in the CMC. It has been previously shown that increasing the salt concentration and decreasing the pH cause the CMC to decrease;<sup>47,48,54,55</sup> therefore, the slightly lower concentration of DPC required to induce a conformational change for both peptides at pH 4.6 is likely a result of the higher salt concentration and/or the low pH. However, the possibility that the MPER peptides exhibit pH-dependent conformational changes cannot be ruled out, similar to the case with FL. Interestingly, the SDS-induced conformational transitions were observed at surfactant concentrations much lower than the CMC. It is therefore possible that the monomeric detergent induces conformational effects of S-MPER and Z-MPER, perhaps by preventing the collapse of hydrophobic groups that would be preferred in pure aqueous solutions.

2D HSQC NMR studies revealed that residues 644–651 interact with DPC and adopt a more helical conformation upon DPC binding. Interestingly, these results are in agreement with the CD spectra observed in 60% TFE. When 60% TFE was added to S-MPER, the amplitude at 220 nm intensified but the 200 nm peak intensity did not change significantly, unlike spectra observed when SDS or DPC was added. Partial structuring in the presence of TFE is consistent with the conclusions based on NMR in DPC micelles that indicate only the C-terminal portion of S-MPER is prone to helix formation in less polar environments. Taken together, these data suggest that S-MPER has some helical propensity in water but contains significant helical content only in the presence of surfactants. These data support an earlier study of an EBOV-derived peptide, EBO<sub>C</sub>, that is composed of the 10 C-terminal residues of Z-MPER and the first six residues of the TM region.<sup>31</sup> FTIR data from this work estimated the 18-residue EBO<sub>C</sub> to be 80% helical, suggesting that 14 residues form an  $\alpha$ -helix. The first four residues of EBO<sub>C</sub> were shown by our NMR analysis of S-MPER to lack secondary structure, implying that it is the region we have identified as helical, with the TM region, that forms a helix.

FIV, the feline immunodeficiency virus, is a lentivirus that has a pathogenesis and entry mechanism similar to that of HIV-1. It has been shown that the FIV MPER has inhibitory activity against FIV. The rationale for this inhibitory activity is that the MPER peptide associates with the target cell membrane and interacts with the fusion peptide, blocking interaction with the MPER of the fusion subunit and hence blocking fusion.<sup>26,49,52,55–58</sup> This is reasonable speculation because this has been demonstrated with the HIV-1 C-peptide inhibitor T20. T20 is a peptide representing one of the  $\alpha$ -helical coiled coils and functions by blocking formation of the trimer of hairpins.<sup>57</sup> The HIV-1 MPER was tested for inhibitory activity as well but was less effective.<sup>58</sup> The inhibitory activity of S-

MPER suggests that addition of this peptide is somehow interfering with the viral entry process, possibly in a manner similar to that of T20. It was found for the FIV MPER that a WX<sub>2</sub>WX<sub>2</sub>W motif is required for the membrane interaction responsible for its inhibitory activity.<sup>55</sup> Interestingly, the Ebola virus MPER also contains the WTGW<sub>2</sub>RQW motif, which is strictly conserved among all species.

Although S-MPER had modest antiviral activity, it did not induce leakage from POPC LUVs. This behavior contrasts with that of EBO<sub>C</sub>, which has membrane lytic activity at a [P]:[L] of  $\sim 10^{-2}$ . EBO<sub>C</sub> is longer than the peptides examined here, encompassing six additional C-terminal residues. It is possible that inclusion of this additional segment mediates deep insertion into the lipid bilayer, resulting in membrane lytic activity for EBO<sub>C</sub>. However, the shorter S-MPER and Z-MPER peptides studied here insert more shallowly into membranes with only the Trp face of the nascent helix interacting with the surface of the DPC micelle in the 5-doxyl stearate NMR experiments, and thus while surfactant binding and conformational changes can be detected by CD, fluorescence, and NMR, the insertion into the lipid bilayer is not sufficiently dramatic to result in membrane lytic activity.

Overall, the results presented here indicate that the MPER segments of EBOV and SUDV bind membrane surfaces and that this induces a conformational change in the Trp-rich segment. This behavior is similar to that of the HIV-1 gp41 MPER and, by analogy, suggests a role for the EBOV and SUDV MPER in membrane fusion. A definitive assignment of function for this region would require mutational studies in the context of a pseudovirus entry system. However, a potential role for the MPER is likely not dependent on pH, which contrasts to the pH-dependent membrane activity of the FL and recent studies by our group and others that suggest low pH induces membrane-active conformations in the isolated ectodomain.<sup>30,59,60</sup>

## ■ ASSOCIATED CONTENT

### ● Supporting Information

Analytical HPLC traces of Z-MPER and S-MPER;  $\theta_{\min}$  and  $\theta_{\max}$  values used for normalized CD plots in Figure 3; peptide binding to LUVs; <sup>1</sup>H, <sup>13</sup>C, and <sup>15</sup>N resonance assignments; and <sup>1</sup>H–<sup>13</sup>C and <sup>1</sup>H–<sup>15</sup>N HSQC spectra. This material is available free of charge via the Internet at <http://pubs.acs.org>.

## ■ AUTHOR INFORMATION

### Corresponding Author

\*E-mail: [jon.lai@einstein.yu.edu](mailto:jon.lai@einstein.yu.edu). Phone: (718) 430-8641. Fax: (718) 430-8565.

### Funding

This work was funded by the Albert Einstein College of Medicine, the National Institutes of Health (Grants AI090249 to J.R.L., GM072085 to M.E.G., and AI088027 to K.C.), and the National Science Foundation (Grant CHE1112188 to J.G.).

### Notes

The authors declare no competing financial interest.

## ■ ABBREVIATIONS

EBOV, Ebola virus; SUDV, Sudan virus; RBD, receptor-binding domain; FL, fusion loop; HIV-1, human immunodeficiency virus type 1; MPER, membrane-proximal external region; TM, transmembrane; CD, circular dichroism; NMR, nuclear magnetic resonance; SDS, sodium dodecyl sulfate; DPC,

dodecylphosphocholine; VSV, vesicular stomatitis virus; LUV, large unilamellar vesicles; POPC, 1-palmitoyl-2-oleoylphosphatidylcholine; RESTV, Reston virus; TFE, trifluoroethanol; CMC, critical micelle concentration; [P]:[L], [peptide]:[lipid] ratio.

## REFERENCES

- (1) Kuhn, J. H., Bao, Y., Bavari, S., Becker, S., Bradfute, S., Brister, J. R., Bukreyev, A. A., Chandran, K., Davey, R. A., Dolnik, O., Dye, J. M., Enterlein, S., Hensley, L. E., Honko, A. N., Jahrling, P. B., Johnson, K. M., Kobinger, G., Leroy, E. M., Lever, M. S., Mühlberger, E., Netesov, S. V., Olinger, G. G., Palacios, G., Patterson, J. L., Paweska, J. T., Pitt, L., Radoshitzky, S. R., Saphire, E. O., Smither, S. J., Swanepoel, R., Towner, J. S., van der Groen, G., Volchkov, V. E., Wahl-Jensen, V., Warren, T. K., Weidmann, M., and Nichol, S. T. (2012) Virus nomenclature below the species level: A standardized nomenclature for natural variants of viruses assigned to the family *Filoviridae*. *Arch. Virol.* 155, 2083–2103.
- (2) Sanchez, A., Kiley, M. P., Holloway, B. P., and Auperin, D. D. (1993) Sequence analysis of the Ebola virus genome: Organization, genetic elements, and comparison with the genome of Marburg virus. *Virus Res.* 29, 215–240.
- (3) Feldmann, H., and Geisbert, T. W. (2011) Ebola haemorrhagic fever. *Lancet* 377, 849–862.
- (4) Sanchez, A., Lukwiya, M., Bausch, D., Mahanty, S., Sanchez, A. J., Wagoner, K. D., and Rollin, P. E. (2004) Analysis of human peripheral blood samples from fatal and nonfatal cases of Ebola (Sudan) hemorrhagic fever: Cellular responses, virus load, and nitric oxide levels. *J. Virol.* 78, 10370–10377.
- (5) Sullivan, N., Yang, Z. Y., and Nabel, G. J. (2003) Ebola virus pathogenesis: Implications for vaccines and therapies. *J. Virol.* 77, 9733–9737.
- (6) Harrison, S. C. (2008) Viral membrane fusion. *Nat. Struct. Mol. Biol.* 15, 690–698.
- (7) White, J. M., Delos, S. E., Brecher, M., and Schornberg, K. (2008) Structures and mechanisms of viral membrane fusion proteins: Multiple variations on a common theme. *Crit. Rev. Biochem. Mol. Biol.* 43, 189–219.
- (8) Miller, E. H., and Chandran, K. (2012) Filovirus entry into cells: New insights. *Curr. Opin. Virol.* 2, 206–214.
- (9) Lee, J. E., Fusco, M. L., Hessel, A. J., Oswald, W. B., Burton, D. R., and Saphire, E. O. (2008) Structure of the Ebola virus glycoprotein bound to an antibody from a human survivor. *Nature* 454, 177–182.
- (10) Lee, J. E., and Saphire, E. O. (2009) Ebolavirus glycoprotein structure and mechanism of entry. *Future Virol.* 4, 621–635.
- (11) Nanbo, A., Imai, M., Watanabe, S., Noda, T., Takahashi, K., Neumann, G., Halfmann, P., and Kawaoka, Y. (2010) Ebolavirus is internalized into host cells via macropinocytosis in a viral glycoprotein-dependent manner. *PLoS Pathog.* 6, e1001121.
- (12) Chandran, K., Sullivan, N. J., Felbor, U., Whelan, S. P., and Cunningham, J. M. (2005) Endosomal proteolysis of the Ebola virus glycoprotein is necessary for infection. *Science* 308, 1643–1645.
- (13) Wong, A. C., Sandesara, R. G., Mulherkar, N., Whelan, S. P., and Chandran, K. (2010) A forward genetic strategy reveals destabilizing mutations in the Ebolavirus glycoprotein that alter its protease dependence during cell entry. *J. Virol.* 84, 163–175.
- (14) Carette, J. E., Raaben, M., Wong, A. C., Herbert, A. S., Obernosterer, G., Mulherkar, N., Kuehne, A. I., Kransusch, P. J., Griffin, A. M., Ruthel, G., Dal Cin, P., Dye, J. M., Whelan, S. P., Chandran, K., and Brummelkamp, T. R. (2011) Ebola virus entry requires the cholesterol transporter Niemann-Pick C1. *Nature* 477, 340–343.
- (15) Cote, M., Misasi, J., Ren, T., Bruchez, A., Lee, K., Filone, C. M., Hensley, L., Li, Q., Ory, D., Chandran, K., and Cunningham, J. (2011) Small molecule inhibitors reveal Niemann-Pick C1 is essential for Ebola virus infection. *Nature* 477, 344–348.
- (16) Miller, E. H., Obernosterer, G., Raaben, M., Herbert, A. S., Deffieu, M. S., Krishnan, A., Ndungo, E., Sandesara, R. G., Carette, J. E., Kuehne, A. I., Ruthel, G., Pfeffer, S. R., Dye, J. M., Whelan, S. P., Brummelkamp, T. R., and Chandran, K. (2012) Ebola virus entry requires the host-programmed recognition of an intracellular receptor. *EMBO J.* 31, 1947–1960.
- (17) Weissenhorn, W., Carfi, A., Lee, K. H., Skehel, J. J., and Wiley, D. C. (1998) Crystal structure of the Ebola virus membrane fusion subunit, GP2, from the envelope glycoprotein ectodomain. *Mol. Cell* 2, 605–616.
- (18) Malashkevich, V. N., Schneider, B. J., McNally, M. L., Milhollen, M. A., Pang, J. X., and Kim, P. S. (1999) Core structure of the envelope glycoprotein GP2 from Ebola virus at 1.9-Å resolution. *Proc. Natl. Acad. Sci. U.S.A.* 96, 2662–2667.
- (19) Koellhoffer, J. F., Malashkevich, V. N., Harrison, J. S., Toro, R., Bhosle, R. C., Chandran, K., Almo, S. C., and Lai, J. R. (2012) Crystal structure of the Marburg virus GP2 core domain in its postfusion conformation. *Biochemistry* 51, 7665–7675.
- (20) Floyd, D. L., Ragains, J. R., Skehel, J. J., Harrison, S. C., and van Oijen, A. M. (2008) Single-particle kinetics of influenza virus membrane fusion. *Proc. Natl. Acad. Sci. U.S.A.* 105, 15382–15387.
- (21) Salzwedel, K., West, J. T., and Hunter, E. (1999) A conserved tryptophan-rich motif in the membrane-proximal region of the human immunodeficiency virus type 1 gp41 ectodomain is important for Env-mediated fusion and virus infectivity. *J. Virol.* 73, 2469–2480.
- (22) Lay, C. S., Ludlow, L. E., Stapleton, D., Bellamy-McIntyre, A. K., Ramsland, P. A., Drummer, H. E., and Pombourios, P. (2011) Role for the terminal clasp of HIV-1 gp41 glycoprotein in the initiation of membrane fusion. *J. Biol. Chem.* 286, 41331–41343.
- (23) Liu, J., Deng, Y., Dey, A. K., Moore, J. P., and Lu, M. (2009) Structure of the HIV-1 gp41 membrane-proximal ectodomain region in a putative prefusion conformation. *Biochemistry (Moscow, Russ. Fed.)* 48, 2915–2923.
- (24) Peisajovich, S. G., Epand, R. F., Pritsker, M., Shai, Y., and Epand, R. M. (2000) The polar region consecutive to the HIV fusion peptide participates in membrane fusion. *Biochemistry* 39, 1826–1833.
- (25) Epand, R. F., Sayer, B. G., and Epand, R. M. (2005) The tryptophan-rich region of HIV gp41 and the promotion of cholesterol-rich domains. *Biochemistry* 44, 5525–5531.
- (26) Reuven, E. M., Dadon, Y., Viard, M., Manukovsky, N., Blumenthal, R., and Shai, Y. (2012) HIV-1 gp41 transmembrane domain interacts with the fusion peptide: Implication in lipid mixing and inhibition of virus-cell fusion. *Biochemistry* 51, 2867–2878.
- (27) Sun, Z. Y., Oh, K. J., Kim, M., Yu, J., Brusica, V., Song, L., Qiao, Z., Wang, J. H., Wagner, G., and Reinherz, E. L. (2008) HIV-1 broadly neutralizing antibody extracts its epitope from a kinked gp41 ectodomain region on the viral membrane. *Immunity* 28, 52–63.
- (28) Song, L., Sun, Z. Y., Coleman, K. E., Zwick, M. B., Gach, J. S., Wang, J. H., Reinherz, E. L., Wagner, G., and Kim, M. (2009) Broadly neutralizing anti-HIV-1 antibodies disrupt a hinge-related function of gp41 at the membrane interface. *Proc. Natl. Acad. Sci. U.S.A.* 106, 9057–9062.
- (29) Noah, E., Biron, Z., Naider, F., Arshava, B., and Anglister, J. (2008) The membrane proximal external region of the HIV-1 envelope glycoprotein gp41 contributes to the stabilization of the six-helix bundle formed with a matching N' peptide. *Biochemistry* 47, 13602–13611.
- (30) Gregory, S. M., Harada, E., Liang, B., Delos, S. E., White, J. M., and Tamm, L. K. (2011) Structure and function of the complete internal fusion loop from Ebolavirus glycoprotein 2. *Proc. Natl. Acad. Sci. U.S.A.* 108, 11211–11216.
- (31) Saez-Cirion, A., Gomara, M. J., Agirre, A., and Nieva, J. L. (2003) Pre-transmembrane sequence of Ebola glycoprotein. Interfacial hydrophobicity distribution and interaction with membranes. *FEBS Lett.* 533, 47–53.
- (32) Han, Z., Licata, J. M., Paragas, J., and Harty, R. N. (2007) Permeabilization of the plasma membrane by Ebola virus GP2. *Virus Genes* 34, 273–281.
- (33) Hwang, T. L., and Shaka, A. J. (1995) Water suppression that works: Excitation sculpting using arbitrary wave-forms and pulsed-field gradients. *J. Magn. Reson., Ser. A* 112, 275–279.

- (34) Kazimierczuk, K., and Orekhov, V. Y. (2011) Accelerated NMR spectroscopy by using compressed sensing. *Angew. Chem., Int. Ed.* 50, 5556–5559.
- (35) Delaglio, F., Grzesiek, S., Vuister, G. W., Zhu, G., Pfeifer, J., and Bax, A. (1995) NMRPipe: A multidimensional spectral processing system based on UNIX pipes. *J. Biomol. NMR* 6, 277–293.
- (36) Vranken, W. F., Boucher, W., Stevens, T. J., Fogh, R. H., Pajon, A., Llinas, M., Ulrich, E. L., Markley, J. L., Ionides, J., and Laue, E. D. (2005) The CCPN data model for NMR spectroscopy: Development of a software pipeline. *Proteins* 59, 687–696.
- (37) Schwarzing, S., Kroon, G. J., Foss, T. R., Wright, P. E., and Dyson, H. J. (2000) Random coil chemical shifts in acidic 8 M urea: Implementation of random coil shift data in NMRView. *J. Biomol. NMR* 8, 43–48.
- (38) Wishart, D. S., Bigam, C. G., Yao, J., Abildgaard, F., Dyson, J. H., Oldfield, E., Markley, J. L., and Sykes, B. D. (1995)  $^1\text{H}$ ,  $^{13}\text{C}$  and  $^{15}\text{N}$  chemical shift referencing in biomolecular NMR. *J. Biomol. NMR* 6, 135–140.
- (39) Marsh, J. A., Singh, V. K., Jia, Z., and Forman-Kay, J. D. (2006) Sensitivity of secondary structure propensities to sequence differences between  $\alpha$ - and  $\gamma$ -synuclein: Implications for fibrillation. *Protein Sci.* 15, 2795–2804.
- (40) Garrett, D. S., Seok, Y. J., Peterkofsky, A., Clore, G. M., and Gronenborn, A. M. (1997) Identification by NMR of the binding surface for the histidine-containing phosphocarrier protein HPr on the N-terminal domain of enzyme I of the *Escherichia coli* phosphotransferase system. *Biochemistry* 36, 4393–4398.
- (41) Miller, E. H., Harrison, J. S., Radoshitzky, S. R., Higgins, C. D., Chi, X., Dong, L., Kuhn, J. H., Bavari, S., Lai, J. R., and Chandran, K. (2011) Inhibition of Ebola virus entry by a C-peptide targeted to endosomes. *J. Biol. Chem.* 286, 15854–15861.
- (42) Stewart, J. C. (1980) Colorimetric determination of phospholipids with ammonium ferrioxalate. *Anal. Biochem.* 104, 10–14.
- (43) Wang, F., Qin, L., Wong, P., and Gao, J. (2011) Facile synthesis of tetrafluorotyrosine and its application in pH triggered membrane lysis. *Org. Lett.* 13, 236–239.
- (44) Wang, F., Qin, L., Pace, C. J., Wong, P., Malonis, R., and Gao, J. (2012) Solubilized gramicidin A as potential systemic antibiotics. *ChemBioChem* 13, 51–55.
- (45) Kim, M. K., and Kang, Y. K. (1999) Positional preference of proline in  $\alpha$ -helices. *Protein Sci.* 8, 1492–1499.
- (46) Buck, M. (1998) Trifluoroethanol and colleagues: Cosolvents come of age. Recent studies with peptides and proteins. *Q. Rev. Biophys.* 31, 297–355.
- (47) Emerson, M. F., and Holtzer, A. (1967) On the ionic strength dependence of micelle number. II. *J. Phys. Chem.* 71, 1898–1907.
- (48) Palladino, P., Rossi, F., and Ragone, R. (2010) Effective critical micellar concentration of a zwitterionic detergent: A fluorimetric study on n-dodecyl phosphocholine. *J. Fluoresc.* 20, 191–196.
- (49) Esposito, C., D'Errico, G., Armenante, M. R., Giannecchini, S., Bendinelli, M., Rovero, P., and D'Ursi, A. M. (2006) Physicochemical characterization of a peptide deriving from the glycoprotein gp36 of the feline immunodeficiency virus and its lipoylated analogue in micellar systems. *Biochim. Biophys. Acta* 1758, 1653–1661.
- (50) Callis, P. R., and Liu, T. (2004) Quantitative prediction of fluorescence quantum yields for tryptophan in proteins. *J. Phys. Chem. B* 108, 4248–4259.
- (51) Giannecchini, S., Di Fenza, A., D'Ursi, A. M., Matteucci, D., Rovero, P., and Bendinelli, M. (2003) Antiviral activity and conformational features of an octapeptide derived from the membrane-proximal ectodomain of the feline immunodeficiency virus transmembrane glycoprotein. *J. Virol.* 77, 3724–3733.
- (52) Apellaniz, B., Ivankin, A., Nir, S., Gidalevitz, D., and Nieva, J. L. (2011) Membrane-proximal external HIV-1 gp41 motif adapted for destabilizing the highly rigid viral envelope. *Biophys. J.* 101, 2426–2435.
- (53) Woody, R. W. (1994) Contributions of tryptophan side chains to the far-ultraviolet circular dichroism of proteins. *Eur. Biophys. J.* 23, 253–262.
- (54) Rahman, A., and Brown, C. W. (1983) Effect of pH on the critical micelle concentration of sodium dodecyl sulphate. *J. Appl. Polym. Sci.* 28, 1331–1334.
- (55) Corrin, M. L., and Harkins, W. D. (1947) The effect of salts on the critical concentration for the formation of micelles in colloidal electrolytes. *J. Am. Chem. Soc.* 69, 683–688.
- (56) D'Errico, G., Vitiello, G., D'Ursi, A. M., and Marsh, D. (2009) Interaction of short modified peptides deriving from glycoprotein gp36 of feline immunodeficiency virus with phospholipid membranes. *Eur. Biophys. J.* 38, 873–882.
- (57) Ingallinella, P., Bianchi, E., Ladwa, N. A., Wang, Y. J., Hrin, R., Veneziano, M., Bonelli, F., Ketas, T. J., Moore, J. P., Miller, M. D., and Pessi, A. (2009) Addition of a cholesterol group to an HIV-1 peptide fusion inhibitor dramatically increases its antiviral potency. *Proc. Natl. Acad. Sci. U.S.A.* 106, 5801–5806.
- (58) Ingale, S., Gach, J. S., Zwick, M. B., and Dawson, P. E. (2010) Synthesis and analysis of the membrane proximal external region epitopes of HIV-1. *J. Pept. Sci.* 16, 716–722.
- (59) Harrison, J. S., Higgins, C. D., Chandran, K., and Lai, J. R. (2011) Designed protein mimics of the Ebola virus glycoprotein GP2  $\alpha$ -helical bundle: Stability and pH effects. *Protein Sci.* 20, 1587–1596.
- (60) Brecher, M., Schornberg, K. L., Delos, S. E., Fusco, M. L., Saphire, E. O., and White, J. M. (2012) Cathepsin cleavage potentiates the Ebola virus glycoprotein to undergo a subsequent fusion-relevant conformational change. *J. Virol.* 86, 364–372.